FLIGHT SIMULATOR TESTING TO ENHANCE COMPREHENSION AND MODELING OF ROTORCRAFT PILOT COUPLINGS

Andrea Zanoni*, Matteo Zago, Rita Paolini, Giuseppe Quaranta, Pierangelo Masarati, Manuela Galli
Politecnico di Milano, Milano - Italy
*andrea.zanoni@polimi.it

Giorgio Maisano
Leonardo Helicopter Division, Cascina Costa - Italy

Lorenzo Frigerio,
Line Up Aviation, Somma Lombardo - Italy

Michal Murawa,
Poznan University of Physical Education, Poznan, Poland

Abstract

The results of a pilot-in-the-loop flight simulator test campaign, aimed at enhancing the comprehension of the interaction between the pilot biomechanical response and the rotorcraft dynamics, are presented. Biomechanical properties – upper limbs motion and electromiographic activities of the most involved muscles – of a test pilot involved in the complex task of ship deck landing, in varying sea conditions and with different helicopter configurations, have been measured. The analysis of the collected data highlights the dependence of the muscular activity on the perceived workload ratings (Bedford scale), and with the approaching of the most challenging portion of the simulated mission, namely the moving deck landing. Several fallbacks on numerical multibody modeling of the biomechanical behavior of the rotorcraft pilot are discussed, in the view of enhancing the quality of prediction of rotorcraft-pilot coupling phenomena.

1 INTRODUCTION

Pilots interact with the helicopter both actively, through their voluntary actions on the control inceptors, and passively, transmitting the accelerations they receive from the seat, through their bodies, back to the inceptors (see Figure 1). The latter transmission path can lead to the generation of undesired, involuntary inputs due to the excitation of some biomechanical modes of vibration of the portion of the pilot body involved in piloting task: as it pertains to the cyclic and collective pitch control inceptors, they can be identified in the upper body, consisting of the torso (including the head) and the upper limbs.

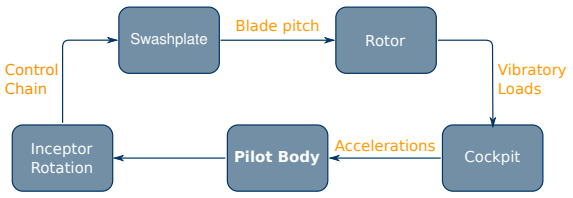

Figure 1: Rotorcraft-pilot inadvertent coupling through the control system

In some cases, the unwanted input can lead to stability problems that are usually referred to as Pilot Assisted Oscillations (PAO), under the comprehensive term Rotorcraft Pilot Couplings (RPC) [1].

The authors are involved (see for example [2, 3]) in an ongoing research effort to study the biodynamics of rotorcraft pilots, aimed at developing prediction and analysis capabilities with respect to the two most important aspects describing the potential adverse interaction [4]:

- the biodynamic feedthrough (BDFT), i.e. the function relating, in the frequency domain, the unwanted command input to the acceleration felt by the pilot body at the interface with the vehicle;
- the neuromuscular admittance (NMA), i.e. the input-output relationship between the joint torques, produced by the muscular activity, and state of the limb.

Clearly, the BDFT depends on the NMA.

The authors' focus, in their contribution to the ongoing research effort, is primarily on numerical modeling, following as much as possible a first-principles approach. Therefore, accurate multibody modeling the biomechanical behavior of the human body has been a constant priority. Multibody biomechanical models of the upper limb and the spine have been developed [2, 5] and have already provided

Presented at the 45th European Rotorcraft Forum, Warsaw, Poland, 17-20 September, 2019

useful insight into the RPC phenomena, e.g. in establishing the dependence of the BDFT on the NMA [6, 7] and of the NMA from the pilot's biodynamic parameters [8].

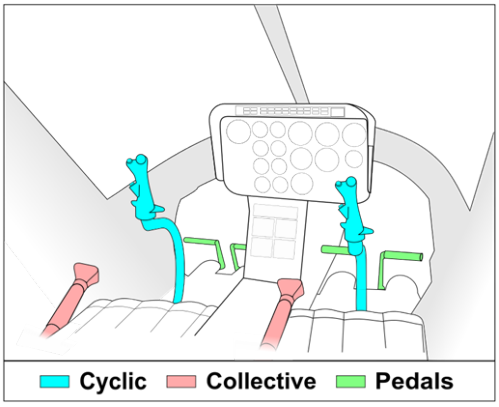

Figure 2: Schematic view of helicopter control inceptors.

Recently, a test campaign has been carried out to collect biodynamic data useful to further enhance and validate the numerical models and to investigate the dependence between pilot workload, muscular activation patterns and NMA/BDFT. This paper focuses on the description of a preliminary testing activity and on its early fallbacks on the multibody models.

2 PROBLEM STATEMENT

A key aspect in numerical modeling to estimate the BDFT and NMA of the pilot is the capability to predict muscular activation patterns of human subjects while performing realistic tasks in a realistic (or "ecologic") environment. In [2], it is postulated that the equivalent stiffness and damping of muscle bundles, whose force is a nonlinear function of muscular elongation and elongation rate as well as of activation, may strongly depend on the muscular activation patterns. The latter are very subjective, task and workload dependent.

Furthermore, since very often multiple muscle pairs actuate the motion of the articular joint they act upon in an agonist/antagonist configuration, there are multiple (in principle, infinite) equivalent levels of muscular activations that can produce the same torques about the said joint. However, different levels of equivalent joint stiffness and damping are generally associated with different activation patterns.

The additional activation contributions, which are not able to vary the joints' torques but act on their equivalent mechanical impedance, have been named *Torque-Less Activation Modes* (TLAMs) in [2]. Understanding their relative importance and upon which parameters their contribution depends is thus among the objectives of the current study.
The work has the following goals:

1. identify typical muscular activation patterns from flight simulator testing of professional test pilots while performing realistic maneuvers of increasing gain and workload;
2. investigate the relationship between subjectively perceived and objectively measured pilot workload, and the type and difficulty of the task, in terms of requested precision;
3. validate and improve the high-fidelity pilot biomechanics models that are used for analysis and prediction of BDFT and NMA.

3 EXPERIMENTAL TESTS

The test campaign was performed in a fixed base flight simulator, offering therefore no direct measurement of the pilot BDFT (this part will be the subject of subsequent work). The approach and landing of a medium weight helicopter on the flight deck of a frigate-like ship has been selected. This manoeuvre includes several mission task elements (MTE) of different complexity, precision and expected workload. The workload of the pilot was varied modifying the ship roll and pitch motion according to the sea state, between 0 and 5 (calm and rough, respectively, Douglas scale). The ship had no forward movement in all but several sea state 5 tests, in which it was moving at 12 knots. The ship heading was kept upwind in the vast majority of the tests, and in all of those composing the subset analyzed in this paper. The position of the aircraft center of mass was also modified in order to increase the workload, moving it aft for the most challenging tests.
The typical task is subdivided in the following MTEs (Fig. 3):

- descent from an initial altitude of 400 ft and reduction of forward ground speed from 50 kts to naval unit speed;
- either a straight-in approach or a hovering manoeuvre alongside the naval unit;
- a hovering manoeuvre directly above the landing deck, in which the pilot waits for a quiescence period in the ship motion;
- the landing manoeuvre.

The pilot was asked to perform a straight-in approach or a hover-alongside approach on a test-to-test basis.

The test matrix dataset was determined considering three repetitions of each trial,varying the levels of the above mentioned parameters from trial to trial. Each trial was preceded by some familiarization flights, performed with either no or perfectly rectilinear and uniform ship motion, without any angular motion.

78 trials were performed during the tests. Of those, 44 were retained in the analysis here presented: discarded tests contain non-standard maneuvers performed to evaluate some critical aspect (e.g. precision hovering, simulated failures of flight systems, different approach paths, etc.) that will be the subject of further analysis.

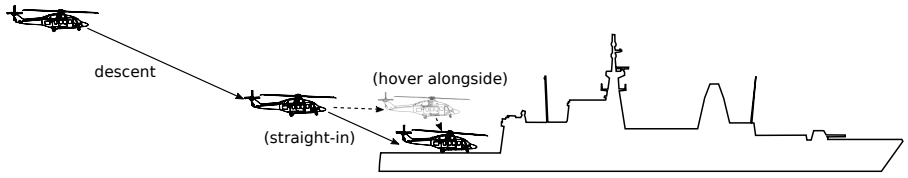

Figure 3: Example of ship-landing maneuvers executed during simulator tests.

In addition to all channels recorded by the flight simulator, a motion capture system was used to reconstruct the motion of the pilot's upper limbs, and a synchronized Surface Electromyography (EMG) system was used to estimate the level of activation of six muscle groups belonging to the shoulder, arm and forearm sections.

Motion Capture

A stereophotogrammetric motion capture system (Smart-D, BTS Bioengineering, Milan, Italy) equipped with 8 cameras placed around and within the rotorcraft simulator recorded at 100 Hz the three-dimensional trajectory of 9 reflective markers (diameter: 15 mm) positioned in the following anatomical landmarks: sternum, left and right acromia, left humerus medial epicondyle, left and right olecrana, left and right ulna styloid process and right radius styloid process (Fig. 4). Three additional markers were positioned on the collective stick of the flight simulator, and used to synchronize motion capture and simulator recordings. The cameras operate in the near infrared (NIR) band; the markers were illuminated appropriately, to avoid interference in the visible band.

Figure 4: Subject with motion capture markers and EMG electrodes, in the configuration used for the tests.

Electromyography

Motor unit EMG signals were measured by surface electrodes (Freemg 1000, BTS Bioengineering, Milano, Italy), integrated in wireless transducers (sampling frequency: 1 kHz). These signals are related to the level of electrical activity of each of the muscle groups they are connected to (Fig. 5). Raw EMG tracks were band-pass filtered and rectified. They were subsequently normalized to the peak activation obtained from three maximum isometric contractions (MVC) performed by the test pilot under the supervision of a professional physiotherapist.

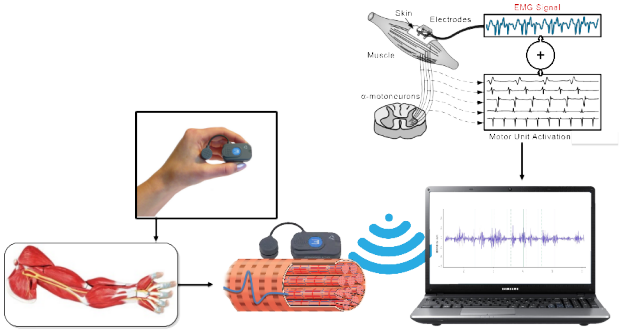

Figure 5: Electromyography: self-contained wireless surface electrodes measure motor unit activation signals.

Transducers were placed on the following muscles according to standard procedures (`http://www.seniam.org/`):

1. *Posterior Deltoid* (shoulder);
2. *Anterior Deltoid* (shoulder);
3. *Triceps Brachii* (arm);
4. *Biceps Brachii* (arm);
5. *Extensor Carpi Radialis* (forearm);
6. *Flexor Carpi Ulnaris* (forearm).

4 MULTIBODY MODELS

The typical approach to BDFT modeling is based on using transfer functions (TF) of the pilot's biodynamics, obtained experimentally, often in flight [1]. However, few relatively sophisticated biomechanical models, yet based on lumped parameters, were developed in the past [9]. The TF approach limits the validity of the analysis to existing cockpit and control inceptor configurations, and hides the influence of the fundamental biomechanics and their intrinsic nonlinearities.

The models used in the present work are implemented in the general-purpose, free multibody analysis software MBDyn (`https://www.mbdyn.org/`) [10], which is also developed by the authors.

The model of each upper limb is composed by six rigid bodies representing the scapula, clavicle, humerus, ulna, radius and hand, constrained by 7 ideal kinematic constraints that model the Sternoclavicular, Acromioclavicular, Glenohumeral, Humeroulnar, Humeroradial, Radioulnar and Radiocarpal joints. The Scapulothoracic joint is modeled through a deformable element. Twenty-eight muscle

bundles act on the remaining 13 degrees of freedom. Each is modeled using a nonlinear viscoelastic element that can be actuated, following the model proposed by Pennestrì et al. in [11], that falls in the general scheme of Hill-type muscular actuators.

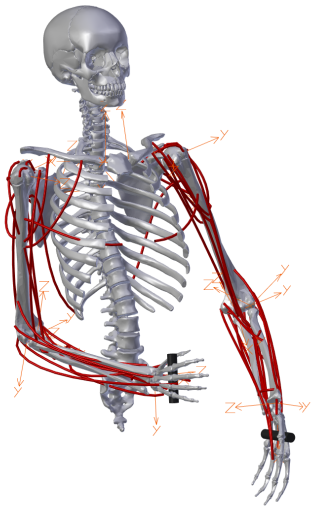

Figure 6: Upper limbs multibody models.

When the motion of the shoulder girdle is discarded, the degrees of freedom of each limb are reduced to 7: the three rotations of the humerus with respect to the torso, the elbow flexion-extension, the forearm prono-supination and the flexion-extension and medio-lateral rotation of the wrist. The muscular fascicles remaining active are 25. The latter is the configuration of the model that has been used in the analyses presented in this work: the motion of clavicle and of the scapula has been deemed negligible with respect to the motion of the remaining limb segments, also in consideration of the fact that piloting tasks do not involve large arm extension angles.
The limb can be considered as a kinematically underdetermined, overactuated manipulator. To cope with the kinematic indeterminacy, the problem is solved directly at the position level. The motion of the degrees of freedom of the model is restrained by “ergonomy” springs, that impose a penalty on the motion of the relative degrees of freedom they connect. Once the complete kinematics of the problem is determined, the joint torques required to produce it can be directly determined using an inverse dynamics problem resolution, since at this level the problem is fully determined. To estimate the corresponding muscular forces, a constrained minimization problem needs to be solved, seeking the activations a_i able to produce the computed joint torques $\mathbf{c}$ through the torques $\mathbf{c}_m$ produced by the muscle actuators, that minimize a cost function (e.g. the total norm of the activation, among the many that have been proposed in the literature) that can vary according to the task, constrained by the admissibility conditions $0 \leq a_i \leq 1$, i.e. the *saturation* limits for the muscle bundles [2]:

$$\min J(\mathbf{a_0}) = \frac{1}{2}\mathbf{a_0}^T \mathbf{W} \mathbf{a_0} \qquad \text{s.t.} \tag{1}$$

$$\mathbf{c} = \mathbf{c}_m \tag{2}$$

$$0 < a_{0i} < 1 \tag{3}$$

The resulting activations are associated with the minimum effort needed to perform the task. To them, a *reflexive* (voluntary) contribution is added, considering a quasi-steady approximation of the activation dynamics, and introducing an activation contribution proportional to the variation of length and contraction velocity of the muscle actuator:

$$a_{r_i} = k_p \left(\frac{x}{x_0} - \frac{x_{\text{ref}}}{x_0} \right) + k_d \left(\frac{\dot{x}}{v_0} \right) \tag{4}$$

this contribution is related to the modulation of the neuromuscular admittance that the nervous system introduces in posture control [12, 13]. Furthermore, from the linearized expression of the relationship between the joint torques and the muscular activations valid at each timestep, some combinations of activations that do not change the overall joint torques but can change the total joint impedance are identified. These represent the *Torque-Less Activation Modes* (TLAMs): a linear combination of these modes can be added to the above mentioned contributions.

These procedures allow for the simulation of entire maneuvers, comprising also the stiffening effect possibly caused by an increased demand for precision in performing the task. The total activation of all the muscle bundles at each timestep is:

$$\mathbf{a} = \mathbf{a}_0 + \mathbf{a}_{\text{TLAM}} + \mathbf{a}_r = \mathbf{a}_0 + \mathbf{K}_{\text{TLAM}}(t)\mathbf{V}_{\text{TLAM}}\mathbf{b} + \mathbf{a}_r \tag{5}$$

where $\mathbf{a}_0$ represents the *baseline* activation, i.e. the minimum required level to produce the torques necessary to perform the piloting task, $\mathbf{a}_{\text{TLAM}}$ the contribution due to TLAMs, and $\mathbf{a}_r$ the reflexive contribution. The TLAMs contribution is added as the linear combination of Torque-Less modes, described by the coefficients b and scaled by the time-dependent gains $\mathbf{K}_{\text{TLAM}}(t)$.

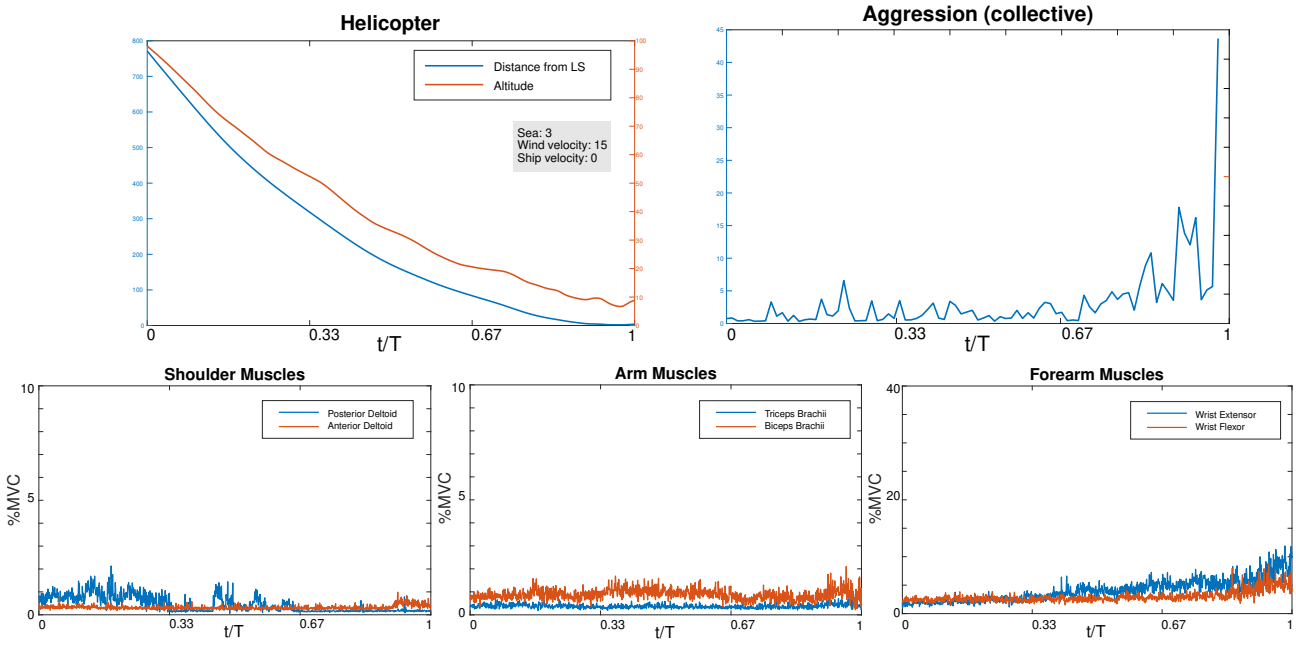

Figure 7: Kinematics (top left), collective and EMG signals (right, from top to bottom) during ship landing.

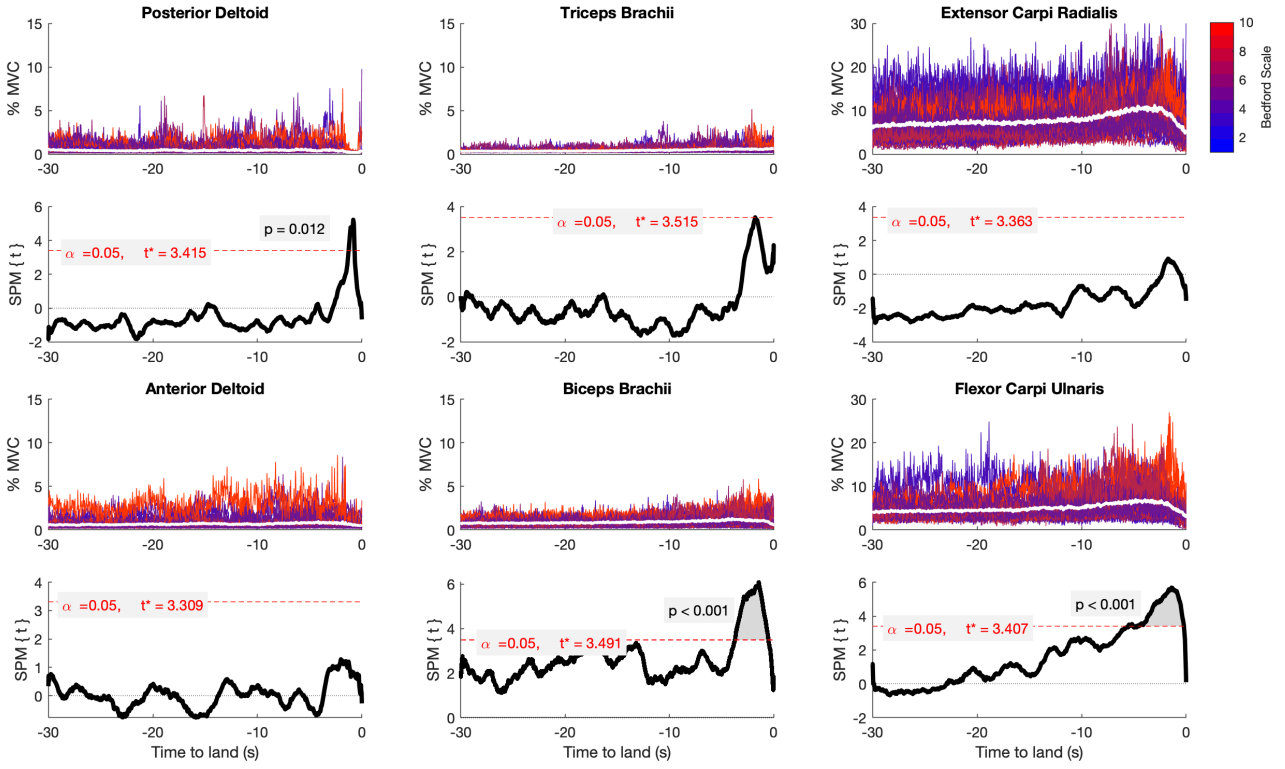

Figure 8: Statistical Parameter Mapping (SPM) analysis of the muscular EMG activities. Correlation has been tested against the Bedford grade of each test.

5 EXPERIMENTAL RESULTS

As mentioned in previous sections, 78 flight simulation tests have been performed, and extensive data processing analysis has been carried out. Results here presented refer to 44 of the the 78 tests, referring to the ones in which no atypical manoeuvres were performed. Workload subjective assessment has been made using the Bedford workload ratings [14] Figure 8 shows the whole EMG dataset and its relationship with the task workload. Muscular activation was fairly low (below 10% MVC) for shoulder and forearm muscles. Rather, values up to 30% MVC were measured at the forearm level. Positive correlations between muscular activation and the Bedford scale ratings were obtained for the Biceps Brachii (a forearm flexor) and the Flexor Carpi Ulnaris approximately between 4 s and 0.5 s before landing.

Statistical approach

Normalized EMG waveforms were obtained for each muscle in the last 30 s preceding the landing instant, identified as the first instant in which all the weight-on-wheels signals were positive and remained positive to the end of the records. The correlation between EMG activation values and the Bedford workload ratings [14] was tested using a statistical parametric mapping (SPM) approach [15]. The scalar output statistics, SPMt, was calculated at each sampling node. SPMt indicates the probability with which a correlation between time series could have been produced by a random field process with the same temporal smoothness. Supra or under threshold clusters indicate the time location of positive or negative correlations, respectively. Further, the Spearman correlation coefficient was used to assess the relationship between the root-mean-square values of EMG activation corresponding to supra/below threshold clusters and the Bedford rate associated. A significance value of $p < 0.05$ was implemented throughout.

Consistently, a moderately positive Spearman correlation ($p < 0.001$) between root-mean-square EMG and the Bedford scale ratings during the same time frames was found (Figure 8)

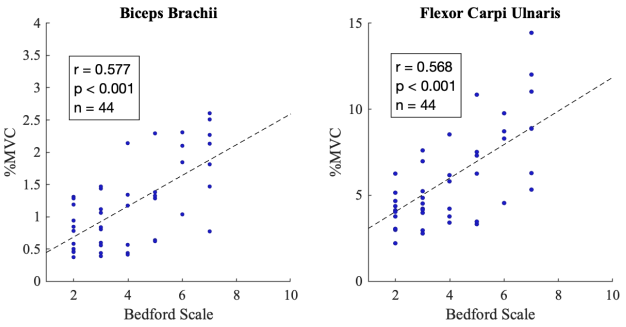

Figure 9: Linear regression between the Bedford scale rating for pilot workload and muscular activations in the Biceps Brachii and the Flexor Carpi Ulnaris. The EMG signal was limited to the portion of the time series in which the SPM analysis indicated the presence of a meaningful statistical correlation.

The increasing precision demand of the selected task while the helicopter approaches the helideck, leading to increasing activation of the muscles, is confirmed by a preliminary inspection of the EMG measurements, as shown in Fig. 7. With reference to Figure 7, some patterns can be noted, and are persistent throughout the tests:

- the EMG signal of forearm muscles is greater than the one of arm and shoulder muscles;
- especially referring to the forearm muscles, the EMG activity grows constantly during the manoeuvre and, especially in the last portion of it, seemingly inversely proportional to the remaining time to land;
- the *average value* of EMG activity of the agonist/antagonist pair of forearm muscles grows as the distance diminished, indicating an increased level of co-contraction, directly responsible for the increase of the equivalent impedance of the wrist joint.

the first point can be specific to the test pilot that was involved in the experimental activity. In other words, it might very well be the product of a specific piloting style. The other two were expected as the primary agent in increasing levels of joint impedance can be identified in higher levels of co-contraction of agonist/antagonist muscle pairs.

In Figure 7, also the value of the aggression calculated on the collective control input following the definition given in [16] is shown. It can be qualitatively noted that, as the mean value of the aggression – meant as a measure of the pilot workload – grows, so do the muscular electrical activities.

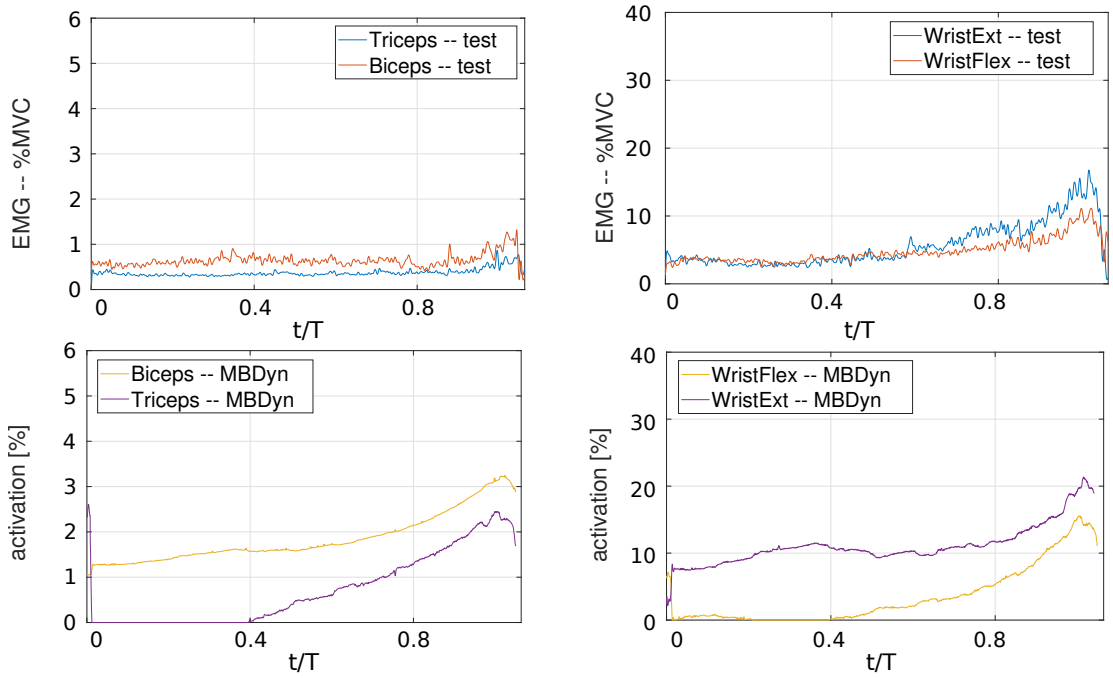

Figure 10: Comparison between EMG signals time histories (top) and computed activation patterns for forearm and arm muscles during a deck landing test. Signals are referred to the nondimensional mission time.

6 FALLBACKS ON MODELING

The existing capability of the multibody models to predict muscular activation through inverse dynamics has been augmented by integrating the motion reconstruction capability through motion capture measurements.

The motion of the markers is imposed to *static* (i.e. having no associated inertia properties) nodes in the multibody model. The markers' nodes are connected to the nodes representing the limbs segments bones though *dummy* elastic elements. The initial location of the markers' nodes is estimated; then, the prestrain of the dummy elastic elements is adjusted to modify the relative location of the markers with respect to the bones, in order to minimize the motion reconstruction error.

Currently, the data analysis of the test measurements is completed for what concerns the "standard" tests, i.e. those in which the main mission task remained that of deck landing strictly from start to end. As discussed in the previous section, some patterns appear evident; therefore, the experimental activity has led to some early modeling fallbacks, that are briefly described in the following sections.

Computation of baseline activation

The choice and weighting of the objective function in the baseline activation computation has been changed to favour the activation of forearm muscles:

$$J(\mathbf{a}_0) = \frac{1}{4}\mathbf{a}_0^T\left(\mathbf{a}_0^T\mathbf{F}_0\mathbf{a}_0\right)\mathbf{a}_0 + \frac{1}{2}\mathbf{a}_0^T\mathbf{F}_0\mathbf{a}_0$$

with $\mathbf{F}_0 = \left[\text{diag}(F_{0i})\right]$, i.e. the peak isometric contraction force of each muscle is used to weight its contribution to the total activation, favoring muscles with smaller F_0, that in the upper limb reside primarily in the forearm section.

Distribution of reflexive activation gains

The distribution of the reflexive activation gains k_p and k_d of equation (4) has been altered to favor the utilization of the forearm muscles in the neuromuscular admittance modulation: each gain has been scaled proportionally to the inverse of the peak isometric contraction force F_{0i}. The resulting distribution, in relative terms, is shown in Figure 11: the gains of the forearm muscles are on average greater than those of the muscles belonging to other limb sections.

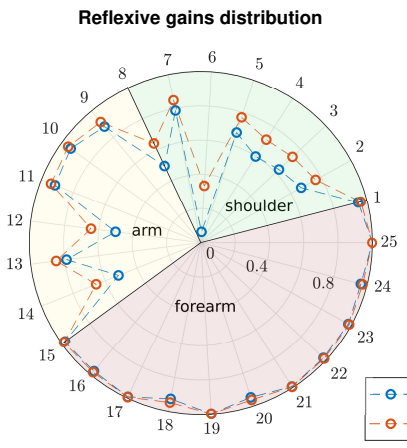

Figure 11: Distribution of proportional gain k_p and derivative gain k_d of reflexive contribution to muscular activation, when scaled proportionally to the inverse of the maximum isometric contraction force F_0. Values are normalized with respect to the reference values $\bar{k}_i = k_i/k_{i,\text{ref}}$ used when they are uniformly distributed.

Gain scheduling using τ-coupling

The use of time-to-target concepts in the prediction of pilot behavior was introduced, starting in 1999, by Gareth Padfield and his group at the University of Liverpool [17]. Their work focuses on the application to aircraft control of concepts originally proposed by Lee [18] in the context of perceptual sciences. In essence, the τ theory postulates that sensory guidance always involves *gap closures* performed by adjusting the closure time, τ, which is a function of the gap distance x and gap closure velocity $\dot{x}$,

$$\tau = \frac{x}{\dot{x}} \tag{6}$$

In the absence of some *extrinsic* motion to couple with, an *intrinsic* guide is created. The strategy used by the pilot during the tests is consistent with a τ-coupling based on the tracking of a constant deceleration guide, at least in the descent and approach phases. In [17], a simple cross-over pilot model originally proposed by Krendal and McRuer in [19] is modified, introducing gain-scheduling derived from τ concepts in the case of constant acceleration or deceleration guides. In particular, the gain K of the cross-over model is given the following time-dependence:

$$K = \frac{2}{kT}(1 - t/T)^{-1} \tag{7}$$

The same time dependence has been used in the present work to modulate the contribution of the TLAMs to the total activation:

$$\mathbf{a} = \mathbf{a}_0 + \mathbf{K}(t/T)\mathbf{V}_{\mathrm{TLAM}}\mathbf{b} + \mathbf{a}_r \tag{8}$$

as shown in Figure 12. The descending portion of the curve has been introduced, subtracting a second inverse-power law, to cope with the decreasing levels of activation that follow the values relative to the initial touch-down.

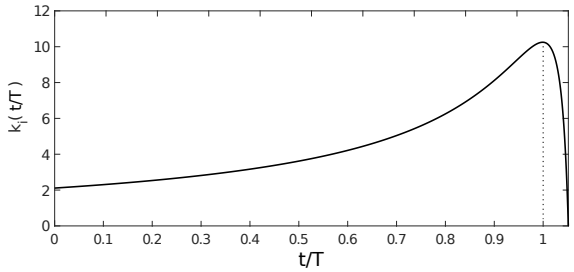

Figure 12: Gain scheduling of the TLAMs contribution to the overall muscle activation, as a function of the nondimensional time to task completion.

Favor TLAMs that increase forearm activation

TLAMs that favour activation level increase in forearm muscles have been favored by weighting the minimum norm objective function

$$J(\mathbf{b}) = \frac{1}{2}\mathbf{b}^T\mathbf{F}_0\mathbf{b}$$

that is minimized to identify the linear combination $\mathbf{b}$ that is eventually added to $\mathbf{a}_0$.

As shown in Figure 10, the combined effect of the above listed interventions has lead to promising enhancements in matching simulation results to measurements.

EFFECTS ON ESTIMATED BDFT

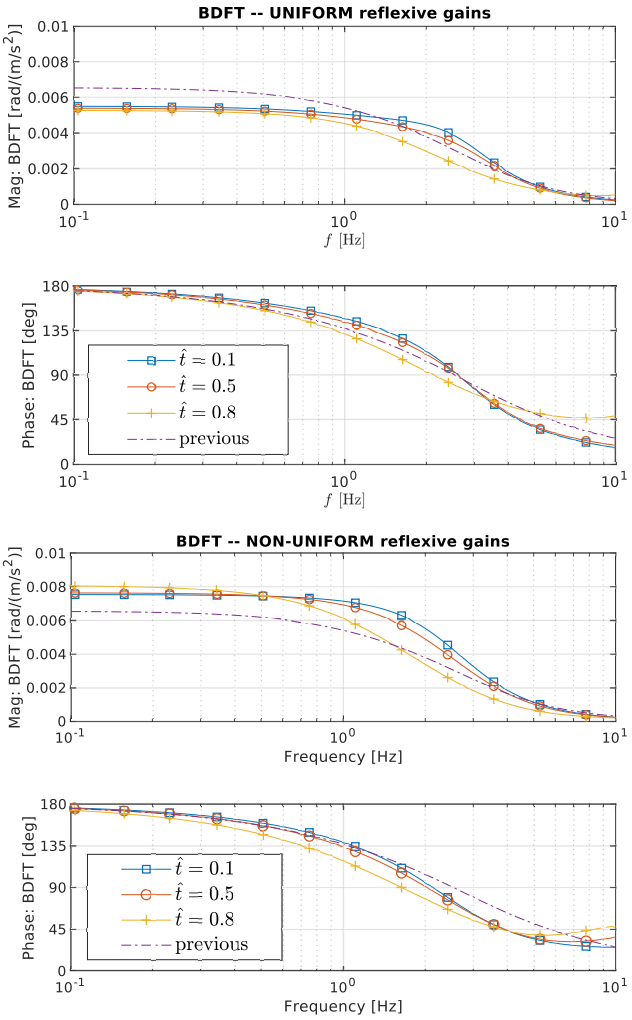

Figure 13: Numerically estimated BDFT functions, with the original multibody model formulation (purple, dash-dot lines), and with the introduced modifications (blue, red and yellow marked lines). The top two graphs refer to the modulus and phase of the BDFT functions obtained, as it pertains to the modified model, without a uniform distribution of the gains of the reflexive contribution to activation. In the bottom two graphs, on the contrary, the distribution of the reflexive gains in the modified model are scaled proportionally to the inverse of the muscles' peak isometric contraction forces, as shown in Figure 11.

The effect of the modifications stemmed from the analysis of the experiments on the collective BDFT estimated through the perturbation of the multibody models about a reference conditions is collected in Figure 11. The BDFT function here

shown is

$$\mathrm{BDFT}(s) = \frac{\Theta_0(s)}{\ddot{Z}_0(s)} \tag{9}$$

i.e. the transfer function between the seat vertical acceleration and the collective lever rotation.

In the top graph, the BDFT obtained with the original model (purple, dash-dot line) is compared with a family of BDFT curves obtained with the modified model, using TLAMs gains according to the curve shown in Figure 12 at different nondimensional mission times $\hat{t} = t/T$, but with a uniform distribution of the gains of the quasi-steady model of the reflexive contribution to activation. In the bottom two graphs, instead, the estimated BDFTs referring to the modified model are obtained using the non-uniform gain distribution of Figure 11. The first conclusion that can be inferred by the results is that both the distribution of the *reference* activation, i.e. the sum of the baseline a_0 and the contribution added through TLAMs, and that of the reflexive portion gains, have an influence on the shape of the BDFT. Considering also the fact the the modifications were suggested by the particular behavior of the pilot that performed the tests, it can be inferred (even if not proved, at the current stage) that the piloting style influences the characteristics of the pilot-rotorcraft also at frequencies associated with involuntary pilot actions on the control inceptors. A second important comment can be made referring to the effect of the varying TLAMs gains: one would expect for an increase of their value to correspond to an increase of the arm equivalent stiffness about the steady configuration, i.e. an increase in the frequency of the biodynamic pole and a reduction of the BDFT static gain. Instead, the opposite trend is found: a sign of the fact that the underlining nonlinearities cannot be discarded to properly investigate RPC phenomena.

7 CONCLUSIONS

The muscular activity of 6 muscles in the forearm, arm and shoulder of an expert helicopter test pilot was measured during 78 flight simulator trials, along with the kinematics of the upper limbs segments, measured through stereophotogrammetry of several reflective markers. The objective of the simulated mission was approach and landing on the flight deck of a frigate-like ship; different sea states and the corresponding effects on the ship motion were simulated in order to vary the pilot workload.

In the 44 homologous tests analyzed in this work, the Surface Electromyography signals showed some common trends: forearm muscles were the most active, with their EMG signals growing during the manoeuvre up until the last instants before touchdown, showing signs of increased co-contraction of agonist/antagonist pairs, especially in the forearm. The EMG signals showed an increase of the level of muscular activity correlated with the task difficulty, as measured by the Bedford workload scale rating given by the pilot at the end of the single test repetition. From the time evolution of the EMG signals, it can be inferred that the pilot is actively controlling the stiffness of the wrist joint, increasing it in the critical segment of the manoeuvre. The results were confirmed through a time-dependent statistical analysis.

Results of the motion capture measures were used to drive simulations of a multibody model of the upper limbs. Early attempts to incorporate the effects of the findings in numerical multibody models of the biomechanical behavior of the pilot upper limbs led to different choices in the figures of merit minimized during the optimization loop dedicated to the estimation of muscular activation, and to a reflexive activation gain-scheduling technique based on the tau (time-to-target) concept.

In the foreseeable future, the authors hope to get a better understanding of the dependence of the activation patterns, and therefore of the BDFTs, from the pilot behavior. For this reason, it is planned to repeat some of the tests with different pilots, especially less experienced ones with the task at hand, or even regular, professional pilot as opposed to test pilots. Another very important aspect that will be the focus of the future work is the experimental validation of the estimated Biodynamic Feedthrough functions.

From the numerical modeling point of view, the next steps are represented by the analysis of the tests that were outside the “standard” test matrix, i.e. those that were performed to highlight particular aspects of the phenomena here involved (i.e., precision hovering tasks).

Copyright Statement

8 Acknowledgments

This work received partial support from Leonardo Helicopter Division. The authors particularly acknowledge LHD, especially in the persons of Andrea Ragazzi, Riccardo Bianco Mengotti and Capt. Andrea Scopa for providing the flight simulator trials and support in collecting the data used in the analysis.

A Muscle actuators

The naming conventions for the muscle actuators in the multibody model is reported in table 1

Label	Name	Section
1	Coracobrachialis	Shoulder
2	Anterior Deltoid	Shoulder
3	Medial Deltoid	Shoulder
4	Posterior Deltoid	Shoulder
5	Latissimus Dorsi	Shoulder
6	Pectoralis Major	Shoulder
7	Supraspinatus	Shoulder
8	Infraspinatus	Shoulder
9	Biceps Caput Longus	Arm
10	Biceps Caput Brevis	Arm
11	Anconeus	Arm
12	Triceps Caput Lateralis/Medialis	Arm
13	Triceps Caput Longus	Arm
14	Brachialis	Arm
15	Brachioradialis	Forearm
16	Pronator Teres	Forearm
17	Flexor Carpi Radialis	Forearm
18	Extensor Carpi Ulnaris	Forearm
19	Extensor Digitorum	Forearm
20	Flexor Digitorum Profundus	Forearm
21	Flexor Carpi Radialis	Forearm
22	Extensor Carpi Radialis	Forearm
23	Pronator Quadratus	Forearm
24	Supinator Brevis	Forearm
25	Abductur Pollicis Longus	Forearm

Table 1: Muscular actuators in the upper limb multibody model.

References

[1] Marilena D. Pavel, Michael Jump, Binh Dang-Vu, Pierangelo Masarati, Massimo Gennaretti, Achim Ionita, Larisa Zaichik, Hafid Smaili, Giuseppe Quaranta, Deniz Yilmaz, Michael Jones, Jacopo Serafini, and Jacek Malecki. Adverse rotorcraft pilot couplings — past, present and future challenges. *Progress in Aerospace Sciences*, 62:1–51, October 2013. doi:10.1016/j.paerosci.2013.04.003.

[2] Pierangelo Masarati, Giuseppe Quaranta, and Andrea Zanoni. Dependence of helicopter pilots' biodynamic feedthrough on upper limbs' muscular activation patterns. *Proc. IMechE Part K: J. Multi-body Dynamics*, 227(4):344–362, December 2013. doi:10.1177/1464419313490680.

[3] Vincenzo Muscarello, Giuseppe Quaranta, and Pierangelo Masarati. The role of rotor coning in helicopter proneness to collective bounce. *Aerospace Science and Technology*, 36:103–113, July 2014. doi:10.1016/j.ast.2014.04.006.

[4] J. Venrooij, M. Mulder, D.A. Abbink, M.M. van Paassen, M. Mulder, F.C.T. van der Helm, and H.H. Bulthoff. Mathematical biodynamic feedthrough model applied to rotorcraft. *Cybernetics, IEEE Transactions on*, 44(7):1025–1038, July 2014. doi:10.1109/TCYB.2013.2279018.

[5] Pierangelo Masarati, Giuseppe Quaranta, and Andrea Zanoni. A detailed biomechanical pilot model for multi-axis involuntary rotorcraft-pilot couplings. In *41st European Rotorcraft Forum*, Munich, Germany, September 1–4 2015.

[6] Pierangelo Masarati and Giuseppe Quaranta. Coupled bioaeroservoelastic rotorcraft-pilot simulation. In *Proceedings of ASME IDETC/CIE*, Portland, OR, August 4–7 2013. DETC2013-12035.

[7] Pierangelo Masarati, Giuseppe Quaranta, Andrea Bernardini, and Giorgio Guglieri. A multibody model for piloted helicopter flight dynamics and aeroservoelasticity. *J. of Guidance, Control, and Dynamics*, 38(3):431–441, 2015. doi:10.2514/1.G000837.

[8] Andrea Zanoni and Vincenzo Muscarello. Moving towards a-priori identification of undesirable pilot biometrics for collective bounce instability. In *43rd European Rotorctaft Forum*, Milano, Italy, September 12–15 2017.

[9] Henry R. Jex and Raymond E. Magdaleno. Biomechanical models for vibration feedthrough to hands and head for a semisupine pilot. *Aviation, Space, and Environmental Medicine*, 49(1–2):304–316, 1978.

[10] Pierangelo Masarati, Marco Morandini, and Paolo Mantegazza. An efficient formulation for general-purpose multibody/multiphysics analysis. *J. of Computational and Nonlinear Dynamics*, 9(4):041001, 2014. doi:10.1115/1.4025628.

[11] E. Pennestrì, R. Stefanelli, P. P. Valentini, and L. Vita. Virtual musculo-skeletal model for the biomechanical analysis of the upper limb. *Journal of Biomechanics*, 40(6):1350–1361, 2007. doi:10.1016/j.jbiomech.2006.05.013.

[12] Pierangelo Masarati and Giuseppe Quaranta. Bioaeroservoelastic analysis of involuntary rotorcraft-pilot interaction. *J. of Computational and Nonlinear Dynamics*, 9(3):031009, July 2014. doi:10.1115/1.4025354.

[13] Sybert Stroeve. Impedance characteristics of a neuromusculoskeletal model of the human arm I. posture control. *Biological Cybernetics*, 81(5–6):475–494, 1999. doi:10.1007/s004220050577.

[14] A. Roscoe and G. Ellis. A subjective rating scale for assessing pilot workload in flight: A decade of practical use. TR 90019, Royal Aerospace Establishment, 1990.

[15] T. C. Pataky, J. Vanrenterghem, and M. A. Robinson. Zero- vs. one-dimensional, parametric vs. non-parametric, and confidence interval vs. hypothesis testing procedures in one-dimensional biomechanical trajectory analysis. *Journal of Biomechanics*, 48(7):1277 – 1285, 2015.

[16] Michael Jones, Michael Jump, and Linghai Lu. Development of the phase-aggression criterion for rotorcraft pilot couplings. *J. of Guidance, Control, and Dynamics*, 36(1):35–47, January-February 2013. doi:10.2514/1.58232.

[17] Gareth Padfield. The tau of flight control. *The Aeronautical Journal*, 115:521–555, 09 2011.

[18] David Lee. A theory of visual control of braking based on information about time-to-collision. *Perception*, 5:437–59, 02 1976.

[19] Duane T. McRuer and Ezra S. Krendel. Mathematical models of human pilot behavior. Paper No. 146, Systems Technology, Inc., 13766 S. Hawthorne Boulevard Hawthorne, California 90250-7083, January 1974. AGARD AG 188.